Water Practice & Technology

IWA PUBLISHING

Water Practice & Technology Vol 17 No 5, 974 doi: 10.2166/wpt.2022.051

Comparing the adsorption isotherms and kinetics of phosphate adsorption on various waste shells as adsorbent

Noorul Hudai Abdullah [a,*], Nur Amirah Adnan[b], Nur Fatin Nadiah Mohd Rashidi[b], Mohamad Syahrul Syazwan Yaacob[c] and Nur Atikah Abdul Salim[d]

[a] Neo Environmental Technology, Centre for Diploma Studies, Universiti Tun Hussein Onn Malaysia, Pagoh Education Hub, 84600, Pagoh, Johor, Malaysia
[b] Centre for Diploma Studies, Universiti Tun Hussein Onn Malaysia, Pagoh Education Hub, 84600, Pagoh, Johor, Malaysia
[c] Faculty of Engineering Technology, Universiti Tun Hussein Onn Malaysia, Pagoh Education Hub, 84600, Pagoh Johor, Malaysia
[d] School of Civil Engineering, Faculty of Engineering, Universiti Teknologi Malaysia, 81310 UTM, Skudai, Johor, Malaysia
*Corresponding author. E-mail: noorul@uthm.edu.my

NHA, 0000-0002-7303-6974

ABSTRACT

Excess phosphate in water bodies causes algae bloom and this phenomenon can reduce the amount of dissolved oxygen in water bodies, resulting in the death of aquatic life. The major focus of this study is to prepare adsorbent from three waste shells for phosphate adsorption from aqueous solution and to compare their effectiveness. This study used adsorbents made from marsh clamshells, waste mussel shells, and eggshells. PO_4^{3-} adsorption by these shells was analysed using several parameter values, with an initial PO_4^{3-} concentration of 10 mg L^{-1}, solution volume of 100 mL, adsorbent dosage of 2 g, and various contact times. The pseudo-second-order kinetic model fitted the batch experimental data better as evidenced by the R^2 values for raw marsh clamshell (0.9991), calcined waste mussel shell (0.9999), and calcined eggshell (0.9997), indicating that the adsorption between the various adsorbents and PO_4^{3-} is a chemisorption process. Calcined eggshell showed the best PO_4^{3-} removal efficiency (99%), followed by calcined waste mussel shell (96%), and raw marsh clamshell (73%). The application of waste material to adsorb phosphate from aqueous solution shows the potential of a new adsorbents for use in real adsorption wastewater treatment technologies.

Key words: eggshell, isotherm model, kinetic model, marsh clamshell, waste mussel shell

HIGHLIGHTS

- The analysis of the experimental data may connect to the kinetic and isotherms modelling.
- This study shows a possible alternative wastewater treatment in tertiary treatment in the field of the wastewater treatment plant.
- The application of waste material to adsorb phosphate from aqueous solution shows the potential for a new low-cost adsorbent for use in real adsorption wastewater treatment technologies.

GRAPHICAL ABSTRACT

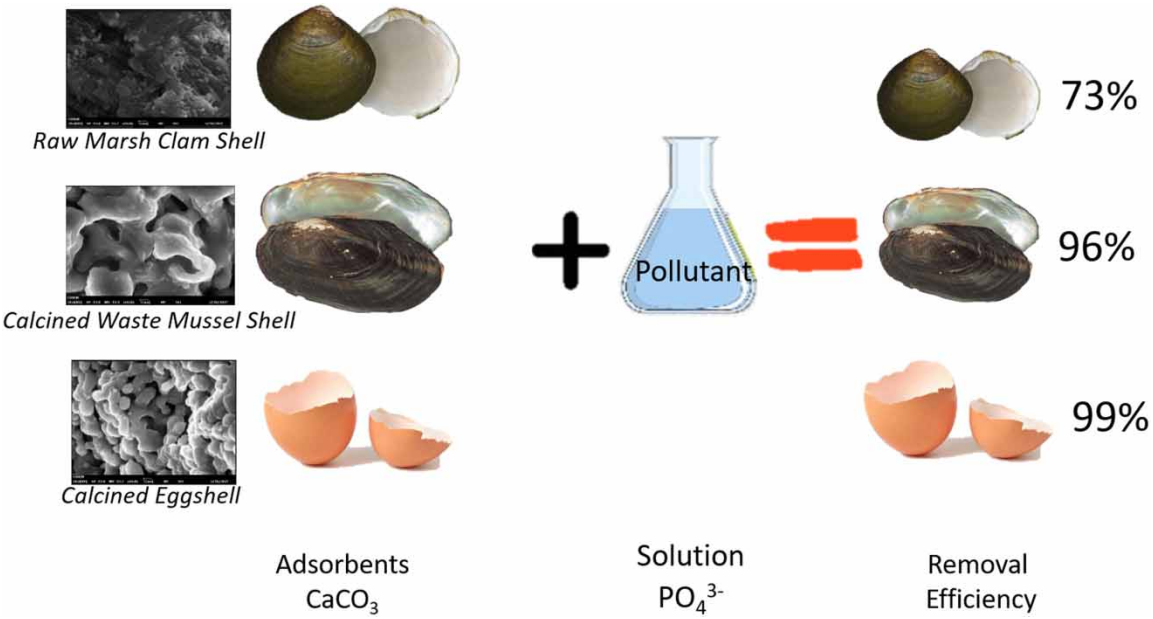

INTRODUCTION

Eutrophication is a main environmental issue globally and has received increased attention in recent decades (Kun *et al.* 2019). Phosphorus (P) is an important nutrient for the growth of biological organisms and algae (Abdul Salim *et al.* 2021a, 2021b). The release of high concentration of P into water bodies is a major cause of eutrophication (Abdul Salim *et al.* 2020). The excess P in water bodies promotes plant growth, reduces water quality, causes algal blooms, and kills aquatic life. The water bodies can also lose their vital functions, resulting in negative consequences to the environment and human health. The three common sources of P in water are polyphosphate, organically bound phosphate, and orthophosphate. Generally, orthophosphates are the most common P compounds found in wastewater (Jibing *et al.* 2011). The European Union (EU) and the United States Environmental Protection Agency (USEPA) have stated that uncontrolled of P release into surface waters may provoke legislation issues. The EU allows a discharge limit of 2 mg L^{-1} per 100,000 population equivalents while the USEPA allows a total phosphorus (TP) effluent limit of less than 0.8 mg L^{-1} (Abdul Salim *et al.* 2018).

Chemical precipitation, biological treatment, membrane separation, and adsorption are some of the phosphorus removal techniques that have been developed in the past few years to treat the excessive amount of P (Huan *et al.* 2021). Among these removal techniques, adsorption is frequently regarded as an excellent and promising approach for removing P from polluted water due to its high efficiency, ease of operation, and economic value (Jung *et al.* 2021; Payel & Animesh 2021). Some of adsorbents come from waste shells with potential to remove P from water due to calcium carbonate contained in the material. The abundance of waste shell produced in domestic usage can caused environmental problems (Tran *et al.* 2021). The use of waste shell, which represents wasted wealth, can give an excellent initiative to sustainability of environment cycle. Marsh clamshell (MCS), waste mussel shell (WMS), and eggshell (ES) are natural adsorbent materials that can be used to remove PO_4^{3-} from wastewater because all of them are waste materials from food processing industries that are normally dumped in foreshores (Nguyen *et al.* 2020; Aravind & Amalanathan 2021). The goal of this study was to investigate the feasibility of using MCS, WMS, and ES as adsorbents to remove PO_4^{3-} from a synthetic solution (KH_2PO_4). The effects of contact time (t) and various particle sizes on the removal of PO_4^{3-} were studied. To investigate the adsorption mechanism, Freundlich and Langmuir isotherm models were used in this study.

METHODS

Adsorbent preparation

MCS, WMS, and ES were used as the adsorbents in this study. The samples were randomly collected from different locations in Malaysia. For the preparation of raw adsorbent, which is MCS, the sample was washed with tap water several times and rinsed using deionised water. The cleaned sample was dried in open air under sunshine for several hours before drying it in an oven at 30 °C for 2 days. The sample was then crushed using mortar and grinder before sieving it to sizes of 1.18, 0.60, 0.30, 0.15, and 0.075 mm. The sieved samples were then weighed and packaged into 2 g per package for each size. For the preparation of calcined adsorbents, which are WMS and ES, the samples were prepared in the same method as MCS. After the sieving process, the samples were calcined in a furnace at 800 °C for 2 h before being weighed and packaged (Nguyen *et al.* 2020).

Synthetic solution

PO_4^{3-} stock solution (100 ppm) was prepared by dissolving 0.1433 g potassium dihydrogen phosphate (KH_2PO_4) in 1 L deionised water and the pH range is 6.6–7.4 with average of pH 7.1. To achieve the required concentration of 10 ppm, the stock solution was diluted with deionised water and then analysed by using an HACH DR6000 UV–vis spectrophotometer to ensure that it can be adopted for the batch experiment (Abdul Salim *et al.* 2020).

Batch experiments

The adsorption isotherm and kinetics were determined by conducting batch experiments. The equilibrium adsorption kinetics and isotherm were examined in batch experiments by adding 2 g of adsorbent from each type (MCS, WMS, and ES) and size (1.18, 0.60, 0.30, 0.15, and 0.075 mm) into a conical flask containing 0.1 L of 10 ppm PO_4^{3-} solution. Ten samples were used for each type and size of adsorbent. Each sample was then shaken at 170 rpm for 30 min, 60 min, 120 min, 180 min, 300 min, 420 min, 1,440 min, 2,880 min, 4,320 min and 5,760 min. Then, the solution was filtered by using a filtration pump. The concentration of PO_4^{3-} in each conical flask was then analysed immediately to determine the removal of phosphorus by using HACH DR6000 UV–vis spectrophotometer. Pseudo-first-order (PFO) and pseudo-second-order (PSO) models were used to determine the adsorption kinetics of PO_4^{3-} onto the adsorbent. The Freundlich and Langmuir isotherm models were applied to analyse the adsorption isotherms of PO_4^{3-} onto MCS, WMS, and ES. The adsorption capacity (q) and the removal efficiency (E) were calculated by using Equations (1) and (2), respectively.

$$q = \frac{(C_i - C_f) \times V}{m} \tag{1}$$

$$E = \frac{(C_i - C_f)}{C_i} \times 100\% \tag{2}$$

where:

C_i – Initial concentration;
C_f – Final concentration;
m – Mass of adsorbent;
V – Volume

Analytical methods

HACH DR6000 UV–vis spectrophotometer was used to measure PO_4^{3-} concentration in the samples using molybdate and amino acid reagents. The surface morphology of MCS, WMS, and ES were observed by using a scanning electron microscope (SEM) (EM-30AX Plus, COXEM, Daejeon, Korea). The chemical compositions of the adsorbents were identified by using energy-dispersive X-ray fluorescence (EDXRF) spectrometer, while BRUKER D2 Phaser benchtop X-ray diffraction (XRD) was used to perform a detailed study of the crystal phase composition of the adsorbents. The functional group of the raw MCS, calcined WMS, and calcined ES were determined by using Fourier transform infrared (FTIR) spectroscopy (Perkin Elmer Spectrum Two FTIR Spectrometer, USA).

Adsorption kinetics model

Adsorption kinetics is useful because it explains the potential rate-controlling step of the adsorption process as well as the true meaning of their observed rate coefficients (Azizian 2004; Liu & Shen 2008). Two types of adsorption kinetic models were used to explain the mechanism of the adsorption process in this study, which are pseudo-first-order (PFO) and pseudo-second-order (PSO) models (Table 1). The PFO equation was used to describe the sorption kinetics and can be written as shown in Table 1 (Ho & McKay 1998; Qiu *et al.* 2009). The PSO kinetic model describes the relationship between the adsorbent's adsorption capacity and time (Edet 2020). The PSO equation can be written as shown in Table 1 (Ho 2006).

Table 1 | List of adsorption kinetics and isotherm models

Models	Linear form	Plot	Parameters
Kinetic			
PFO	$\ln(q_e - q_t) = \ln(q_e) - k_1 t_i$	$\ln(q_e - q_t)$ *vs.* t_i	q_e k_1
PSO	$\frac{t}{q_t} = \frac{1}{k_2 q_e^2} + \frac{t_i}{q_e}$	$\frac{t_i}{q_t}$ *vs.* t_i	q_e k_2
Isotherm			
Freundlich	$\ln q_e = \ln K_F + \frac{1}{n} \ln C_e$	$\ln q_e$ *vs.* $\ln C_e$	K_F n
Langmuir	$\frac{1}{q_e} = \frac{1}{K_L q_{max} C_e} + \frac{1}{q_{max}}$	$\frac{1}{q_e}$ *vs.* $\frac{1}{C_e}$	q_{max} K_L
Nomenclature			
t_i	Adsorption time (min)		
C_e	The concentration of the adsorbate at equilibrium (mg L^{-1})		
q_e	Adsorption capacity at equilibrium (mg g^{-1})		
q_t	Adsorption capacity at time t (mg g^{-1})		
q_{max}	Maximum adsorption capacity (mg g^{-1})		
k_1	PFO rate constant of adsorption (min^{-1})		
k_2	PSO rate constant of adsorption (g mg^{-1} min^{-1})		
K_F	Freundlich constant (mg g^{-1})		
K_L	Adsorption energy coefficient (L mg^{-1})		
n	Heterogeneity factor (dimensionless)		

Adsorption isotherm models

Two adsorption isotherm models are commonly used to explain the adsorption isotherm, namely Freundlich and Langmuir models. According to the Freundlich model, the adsorbates from a heterogeneous surface are formed on the adsorbent's surface through multilayer sorption of different adsorption energies (Nodeh *et al.* 2017). In contrast, the Langmuir model explains monolayer sorption on distinct localised adsorption sites. It assumes uniform energies of monolayer sorption onto the sorbent surface and indicates no adsorbate transmigration in the plane of the surface (Singh *et al.* 2018). The linear form of the Freundlich isotherm model can be written as shown in Table 1 (Efome *et al.* 2018).

According to the Freundlich isotherm, a plot of ln q_e against ln C_e should yield a straight-line intercept at K_F with a slope of 1/n (Table 1). The affinity of the adsorbate–adsorbent is indicated by the adsorption coefficient K_F. The exponent n is related to the adsorbent surface's energetic heterogeneity and determines whether the curve is favourable or unfavourable (Worch 2012). The linear form of the Langmuir isotherm model can be written as shown in Table 1 (Li *et al.* 2013). K_L and q_{max} values represent the Langmuir isotherm constant and maximum adsorption capacity, respectively.

RESULTS AND DISCUSSION

Physicochemical characteristics of adsorbents

EDXRF, SEM, XRD, and FTIR analysis showed the characterisation of raw MCS, calcined WMS, and calcined ES. Figure 1 shows the surface morphology of the shells at 10000× magnification obtained from SEM. Figure 1(a) shows the SEM image of raw MCS that has a compact texture and low porosity (Abdul Salim *et al.* 2021a, 2021b). The SEM micrograph of calcined WMS is shown in Figure 1(b), while Figure 1(c) shows the SEM image of calcined ES. The calcined shells have small pores at the shell surface.

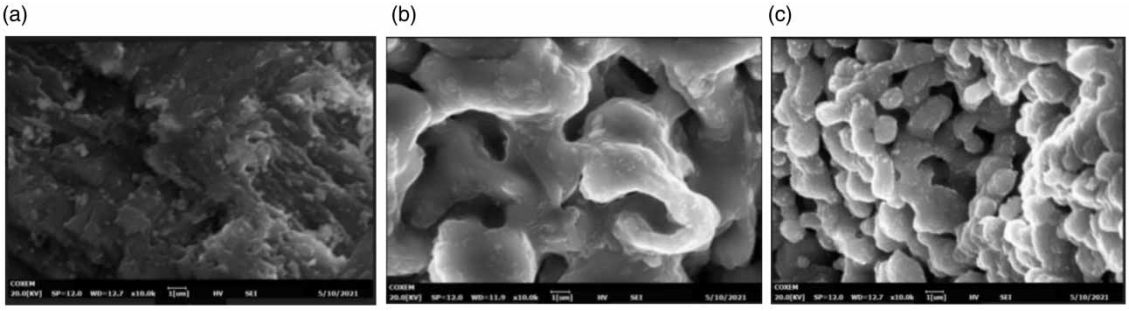

Figure 1 | SEM photomicrograph at 10000× magnification of (a) raw MCS, (b) calcined WMS, and (c) calcined ES.

The elemental compositions of raw MCS, calcined WMS, and calcined ES were examined by EDXRF (EM-30AX Plus, COXEM, Daejeon, Korea). Table 2 shows the elemental composition of raw MCS, calcined WMS, and calcined ES. The major elements in all three shells were Ca and O, in which 27.96% Ca and 55.33% O were measured in raw MCS, 59.74% Ca and 38.92% O in calcined WMS, and lastly, 37.61% Ca and 53.92% O in calcined ES. Normally, materials that contain Ca have the potential to remove PO_4^{3-} from an aqueous solution (Malihe *et al.* 2019). So all three shell varieties have the potential to adsorb PO_4^{3-} from an aqueous solution.

Table 2 | Elemental composition of raw MCS, calcined WMS, and calcined ES type

	Type of adsorbents (weight %)		
Element	**Raw MCS**	**Calcined WMS**	**Calcined ES**
Ca	27.96	59.74	37.61
O	55.33	38.92	53.92
C	15.84	–	5.98
Na	0.56	0.60	0.20
Al	0.08	–	0.27
Fe	0.06	0.28	–
Sr	0.17	0.31	0.15
Mg	–	0.06	1.33
K	–	0.09	0.08
Cu	–	–	0.45

The XRD patterns (refer Table 2) of raw MCS, calcined WMS, and calcined ES were determined by using BRUKER D2 Phaser benchtop XRD instrument. The XRD pattern (refer Figure 2(a)) for raw MCS sample indicates that the major components are aragonite ($CaCO_3$) and calcium carbonate ($CaCO_3$). Next, the XRD pattern of calcined WMS (Figure 2(b)) indicates that lime (CaO) is a major component of calcined WMS. Portlandite ($HCaO_2$), iron (Fe), oxygen (O_2), magnesium (Mg), and strontium cobalt manganese oxide are also present in the XRD pattern of calcined WMS. The EDX pattern of calcined ES (Figure 2(c)) shows that the major component is lime (CaO). The EDX pattern also shows the presence of other components such as portlandite

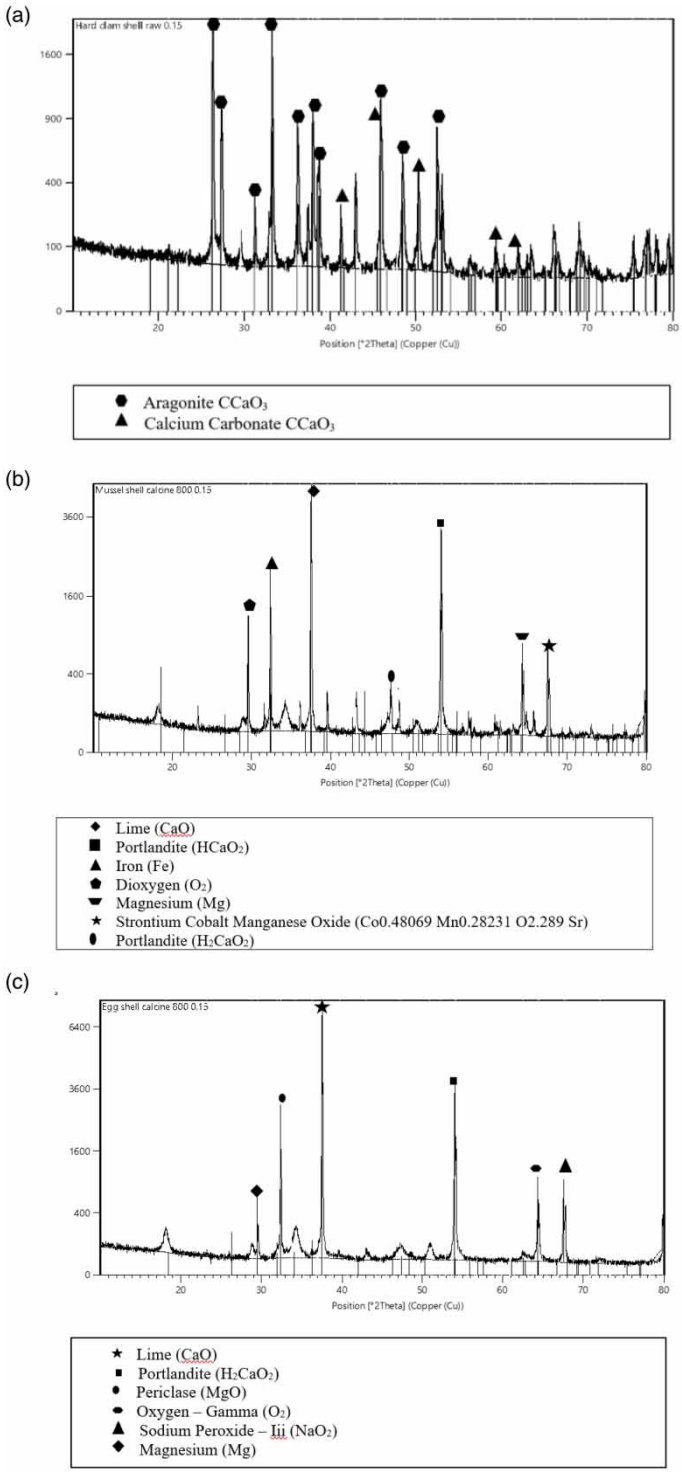

Figure 2 | XRD pattern of (a) raw MCS, (b) calcined WMS, and (c) calcined ES.

(H_2CaO_2), periclase (MgO), oxygen (O_2), sodium peroxide (Na_2O_2), and magnesium (Mg). Other researchers have reported that lime (CaO) and aragonite ($CaCO_3$) have a good phosphate adsorption property (Xie *et al.* 2017).

The functional groups of raw MCS, calcined WMS, and calcined ES were determined by using FTIR spectroscopy (Perkin Elmer Spectrum Two FTIR Spectrometer, USA). The FTIR spectra of raw MCS, calcined WMS, and calcined ES before and after PO_4^{3-} adsorption are listed in Table 3. The difference in frequencies for (a) raw MCS was in the range of −3.37 to 0.11 cm^{-1}, (b) calcined WMS was in range of −2.58 to

Table 3 | FTIR spectra of raw MCS, calcined WMS, and calcined ES before and after adsorption of PO_4^{3-}

Frequency of spectrum (cm^{-1})				
Before adsorption	**After adsorption**	**Differences**	**Detection of functional group**	**References**
Raw MCS				
1,459.36	–	–	C–H bending	Merenda *et al.* (2016), Abdul Salim *et al.* (2021a, 2021b)
–	1455.63	–	C–H bending	
1082.78	1082.89	0.0011	C–O stretching	
857.45	856.92	−0.53	C–H bending	
712.68	712.77	0.09	C = C bending	
699.82	699.93	0.11	C = C bending	
Calcined WMS				
3641.13	3641.64	0.51	O–H stretching	Merenda *et al.* (2016)
1410.29	1407.71	−2.58	S = O stretching	
873.61	872.48	−1.13	C–H bending	
713.1	712.09	−1.01	C = C bending	
Calcine ES				
3645.30	3639.65	5.65	O–H stretching	Merenda *et al.* (2016)
–	3379.56	–	N–H stretching	
1411.22	1418.12	6.9	O–H bending	
1057.4	1058.85	1.45	C–O stretching	
874.19	872.40	1.79	C = C bending	

0.51 cm^{-1}, and (c) calcined ES were the range of 1.45–6.9 cm^{-1}. The position and shape of the PO_4^{3-} stretching band in the FTIR spectra of raw MCS, calcined WMS, and calcined ES are influenced by the nature and position of the surface functional groups (Merenda *et al.* 2016).

The frequencies of raw MCS before PO_4^{3-} adsorption were 1,082.78, 857.45, 712.68, and 699.82 cm^{-1} and significantly changed to 1,082.89, 856.92, 712.77, and 699.93 cm^{-1} after PO_4^{3-} adsorption from synthetic solution. The difference in the frequency spectrum of 0.0011 cm^{-1} (1,082.78–1,082.89 cm^{-1}) was attributed to the CO stretching vibrations (Yuri & Anatoliy 2011). Adsorption of PO_4^{3-} from aqueous solution onto the surface of raw MCS caused a change on the C = C bending frequency spectrum by 0.09 cm^{-1} (712.68–712.77 cm^{-1}) and 0.11 cm^{-1} (699.82–699.93 cm^{-1}) due to the interaction of PO_4^{3-} and C = C functional groups. A change in the C–H bending occurred after PO_4^{3-} adsorption where a new peak was formed at 1,455.63 cm^{-1}; in contrast, the C–H bending was attributed to the 1,459.36 cm^{-1} peak before PO_4^{3-} adsorption.

The FTIR spectra of calcined WMS as shown in Table 3 significantly changed from 3,641.13, 1,410.29, 873.61, and 713.1 cm^{-1} before adsorption to 3,641.64, 1,407.71, 872.48, and 712.09 cm^{-1} after PO_4^{3-} adsorption. The difference of 0.51 cm^{-1} (3,641.13–3,641.64 cm^{-1}) between two spectra was due to the O–H stretching at the surface of calcined WMS being affected by the vibration of the asymmetric stretching mode (Rao 2001). Other than that, the frequency spectrum of S = O stretching had a difference of −2.58 cm^{-1} (1,410.29–1,407.71 cm^{-1}). The frequencies of C–H bending and C = C bending also shifted by −1.13 cm^{-1} (873.61–872.48 cm^{-1}) and −1.01 cm^{-1} (713.1–712.09 cm^{-1}), respectively.

PO_4^{3-} adsorption onto the surface of calcined ES resulted in an increase by 5.65 cm^{-1} (3,645.3–3,639.65 cm^{-1}) on the O–H stretching frequency spectrum, because the interaction between PO_4^{3-} and O–H functional group can affect the vibration asymmetric stretching mode (Gilbert 1999). The band near 1,418.12 cm^{-1} was attributed to O–H bending. The peak at 1,058.85 cm^{-1} corresponded to C–O stretching (Peter 2018). Because of the vibration, this can influence the stretching (Norman *et al.* 1990). A new peak was observed at 3,379.56 cm^{-1} and was associated with the stretching of the N–H functional group (Salim *et al.* 2021).

Adsorption of PO_4^{3-} from a synthetic solution

Figure 3 shows the phosphate removal efficiency by (a) raw MCS, which reached 73, 17, 21, 37, and 62%, while (b) calcined WMS reached 96, 96, 95, 92, and 94% and (c) calcined ES reached 98, 97, 93, 99, and 96% after a

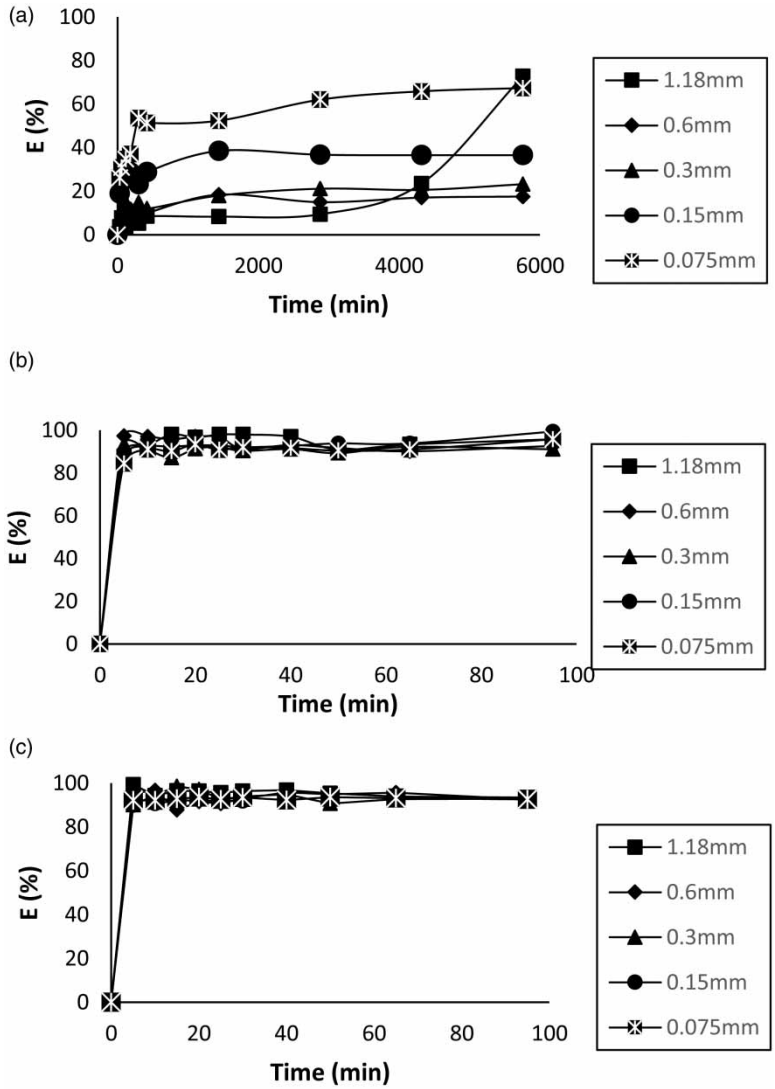

Figure 3 | The efficiency of PO_4^{3-} removal from synthetic solution for (a) raw MCS, (b) calcined WMS, and (c) calcined ES.

contact time of 5,760 min for raw MCS and 95 min for calcined WMS and calcined ES. For raw MCS, the PO_4^{3-} removal efficiency constantly increased for the 30, 60, 120, 180, 300, and 420 min. The increment occurred until a constant value was reached at 420 min as shown in Figure 3(a). The fast adsorption of PO_4^{3-} onto raw MCS during the initial stage was due to the abundance of free active sites on the adsorbent's surface, where it is related to the different SEM analysis on Figure 1 (Leone & Vincenzo 2020). It shows the fastest adsorption on early stage but reducing interaction of PO_4^{3-} due to deficiency of surface area contact (Abdul Salim *et al.* 2020). Figure 3(b) shows the phosphate removal efficiency of calcined WMS. The efficiency increased drastically during the first 5 min and continued to reach equilibrium. The times of equilibrium were 10, 15, 40, and 50 min for the adsorption of phosphate. The rate of phosphate adsorption onto calcined WMS increased because the adsorbent contained many active sites on its surface, where; CaO is major components in adsorbents as mentioned in Table 2 (Suprakas *et al.* 2020). PO_4^{3-} removal efficiency of calcined ES also rapidly increased during the first 5, 10, 15, and 20 min. Then, it slowly increased until it reached equilibrium at 30 min (Figure 3(c)). The availability of many free active sites on the adsorbent surface was the factor of the rapid phosphate adsorption on calcined ES.

Adsorption kinetics

The parameters for the adsorption of PO_4^{3-} onto raw MCS, calcined WMS, and calcined ES fitted to PFO and PSO models are shown in Table 4. To determine the best model for this study, the value of F_e was calculated using Equation (3) (Barakan *et al.* 2020). The most suitable kinetic model for the adsorption should have low

Table 4 | Kinetic parameters from the PFO model for the adsorption of PO_4^{3-} onto raw MCS, calcined WMS, and calcined ES

PFO

Type of adsorbent	Particle size (mm)	$q_{t(theo)}$ (mg g^{-1})	k_1 (min^{-1})	R^2	F_e	$q_{t(exp)}$ (mg g^{-1})
Raw MCS	1.18–2.36	0.4029	0.0001	0.1990	0.3187	0.3675
	0.60–1.18	0.0767	0.0008	0.0314	0.1161	0.0860
	0.30–0.60	0.0762	0.0008	0.5774	0.1775	0.1010
	0.15–0.30	0.0939	0.0009	0.8001	0.5296	0.1770
	0.075–0.15	0.1823	0.0013	0.3373	0.6604	0.3085
Calcined WMS	1.18–2.36	0.0109	0.0098	0.0164	–	0.4810
	0.60–1.18	0.0355	0.0267	0.1649	2.1367	0.4505
	0.30–0.60	0.0606	0.0291	0.2880	–	0.4825
	0.15–0.30	0.0345	0.0625	0.3273	0.9575	0.4875
	0.075–0.15	0.0186	0.0250	0.1648	1.0394	0.4960
Calcined ES	1.18–2.36	0.0664	0.0242	0.2354	–	0.4885
	0.60–1.18	0.0110	−0.0061	0.0075	–	0.4655
	0.30–0.60	0.0372	0.0477	0.3681	4.0941	0.4370
	0.15–0.30	0.1062	0.1824	0.5314	–	0.4425
	0.075–0.15	0.0837	0.9998	0.5157	–	0.4280

F_e value, and the value of R^2 must be close to 1.

$$F_e = \sqrt{\left(\frac{1}{n-p}\right) \cdot \sum_{i}^{n} (q_{t(\exp)} - q_{t(theo)})^2} \tag{3}$$

Tables 4 and 5 show that the correlation coefficient for raw MCS ($R^2 = 0.9991$) for the PSO model was higher than that for PFO model ($R^2 > 0.8001$). Based on the lower F_e value and the R^2 value being near to 1, the PSO model is more suitable than the PFO model to explain the adsorption. For calcined WMS, the best kinetic model is the PSO model, in which the value of R^2 (0.9999) is larger than that of the PFO model ($R^2 = 0.3273$), and it also has a lower F_e value. For the calcined ES, the more suitable kinetic model is also the PSO model ($R^2 = 0.9997$), which has a higher correlation coefficient than the PFO model ($R^2 = 0.5314$) and lower F_e value. The adsorption process in this study can be classified as chemisorption because of the exchange of adsorbent and aqueous solution (Boyd *et al.* 1947).

Table 5 | Kinetic parameters from the PSO model for the adsorption of PO_4^{3-} onto raw MCS, calcined WMS, and calcined ES

PSO

Type of adsorbent	Particle size (mm)	q_e (theo) (mg g^{-1})	k_2 (g mg^{-1} min^{-1})	R^2	Fe	q_e (exp) (mg g^{-1})
Raw MCS	1.18–2.36	0.4051	0.0005	0.1847	1.2620	0.3675
	0.60–1.18	0.0893	0.0626	0.9903	0.1234	0.0860
	0.30–0.60	0.1086	0.0539	0.9925	0.1592	0.1010
	0.15–0.30	0.1783	0.1093	0.9991	0.1563	0.1770
	0.075–0.15	0.3353	0.0241	0.9965	0.4187	0.3085
Calcined WMS	1.18–2.36	0.4715	−6.7295	0.9996	–	0.4810
	0.60–1.18	0.4408	30.7623	0.9992	0.0568	0.4505
	0.30–0.60	0.4715	−6.7295	0.9996	–	0.4825
	0.15–0.30	0.4919	9.4938	0.9998	0.0187	0.4875
	0.075–0.15	0.4912	−38.6251	0.9999	0.0157	0.4960
Calcined ES	1.18–2.36	0.4652	−5.3698	0.9985	–	0.4885
	0.60–1.18	0.4376	−4.7927	0.9994	–	0.4655
	0.30–0.60	0.4368	18.4946	0.9997	0.3082	0.4370
	0.15–0.30	0.4689	1.8751	0.9982	–	0.4425
	0.075–0.15	0.4443	2.9372	0.9987	–	0.4280

Adsorption isotherms

The experimental data were also fitted to the Langmuir and Freundlich models for the analysis of the adsorption isotherm of PO_4^{3-} onto raw MCS, calcined WMS, and calcined ES. All the values of the parameters calculated using these two isotherm models are shown in Table 6. The experimental data are better fitted to the Freundlich isotherm model compared to Langmuir isotherm model, in which the R^2 is close to 1. The R^2 for raw MCS in the Freundlich model is better (0.9491) compared to that of the Langmuir model. It is the same with calcined WMS and calcined ES, in that the correlation is fitted better with $R^2 = 0.3965$ and $R^2 = 0.9377$, respectively as shown in Figure 4.

Table 6 | The parameters from Freundlich and Langmuir models for adsorption of PO_4^{3-} onto raw MCS, calcined WMS, and calcined ES

	Freundlich model			Langmuir model		
Type of adsorbent	**n**	**K_F (mg g^{-1})**	**R^2**	**q_{max} (mg g^{-1})**	**K_L (L mg^{-1})**	**R^2**
Raw MCS	−0.7514	1.6120	0.9491	0.0732	0.4049	0.7702
Calcined WMS	15.8982	0.4986	0.3965	0.5118	28.8596	0.3810
Calcined ES	−13.3690	0.4277	0.9377	0.4888	5.7292	0.9217

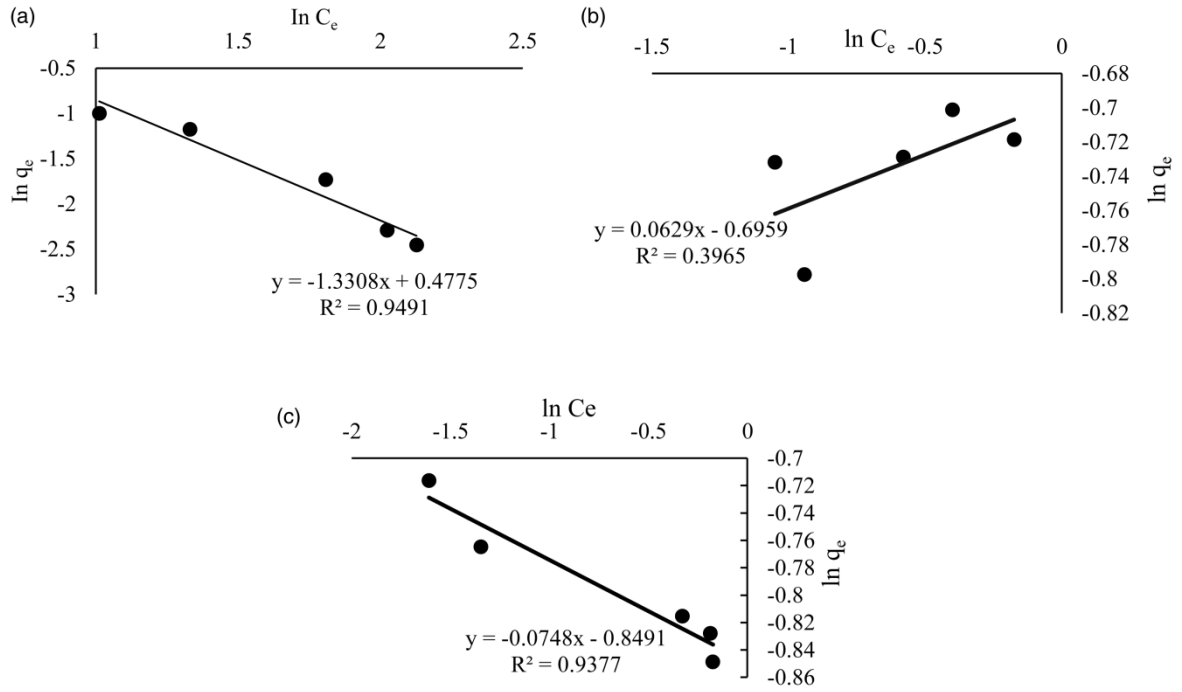

Figure 4 | Adsorption isotherms for (a) raw MCS, (b) calcined WMS, and (c) calcined ES.

The outcome shows that all three shells can adsorb PO_4^{3-} from the synthetic solution. This is because the affinity between calcium oxide present on the surfaces of raw MCS, calcined WMS, and calcined ES and phosphate ions is quite strong since both compounds have different charges, causing them to attract each other (Barry & James 2016). Figure 2 shows the PO_4^{3-} adsorption efficiency rates onto calcined WMS and calcined ES were better and only took 95 min to reach the equilibrium point, compared to the PO_4^{3-} adsorption onto raw MCS, which took a long period to reach the equilibrium point (Mengyuan *et al.* 2021). This is because the calcination process produces a change in calcium carbonate and altered the physical and chemical properties of the WMS and ES. Calcium carbonate changes to calcium oxide at 600–800 °C (Rafia *et al.* 2021). This is supported by Figure 1 that shows the difference between the porosity of the calcined WMS and calcines ES with the raw MCS. The raw MCS has a compact texture, while calcined WMS and calcined ES have small pores in their structures.

CONCLUSIONS

The feasibility of using MCS, WMS, and ES as an adsorbent to remove PO_4^{3-} from synthetic solution was investigated. The adsorption kinetics data of MCS, WMS, and ES fitted well with the PSO model with R^2 values of 0.9991, 0.9999, and 0.9997, respectively, indicating that the PO_4^{3-} adsorption on the various adsorbents is a chemisorption process. The adsorption isotherms data of MCS, WMS, and ES fitted well with the Freundlich model, the study shows the PO_4^{3-} adsorption is suitable for MCS and ES. This present study provided more information on the adsorption of phosphate from aqueous solution onto raw MCS, calcined WMS, and calcined ES. The application of waste material to adsorb the phosphate from aqueous solution shows the potential of a new adsorbent for use in real adsorption wastewater treatment technologies.

ACKNOWLEDGEMENT

This research was supported by the Ministry of Higher Education (MOHE) through the Fundamental Research Grant Scheme (FRGS/1/2020/TK0/UTHM/02/22) or Vot No. K308. The authors would also like to thank the Neo Environment Technology (NET), Centre for Diploma Studies (CeDS), Research Management Centre, Universiti Tun Hussein Onn Malaysia for its support.

DATA AVAILABILITY STATEMENT

All relevant data are included in the paper or its Supplementary Information.

REFERENCES

Abdul Salim, N. A., Abdullah, N. H. & Muhammad, R. K. 2018 Adsorption of phosphate from aqueous solutions using waste mussel shell. In *MATEC Web Conf.*, 11 December, Malaysia.

Abdul Salim, N. A., Mohd, H. P. & Abdull, R. M. Y. 2020 Adsorption isotherms and kinetics of phosphate on waste mussel shell. *Malaysian Journal of Fundamental and Applied Sciences* **16**(3), 393–399.

Abdul Salim, N. A., Mohd, H. P. & Abdull, R. M. Y. 2021a Adsorption of phosphate from aqueous solution onto iron-coated waste mussel shell: physicochemical characteristics, kinetic, and isotherm studies. *Biointerface Research in Applied Chemistry* **11**(5), 12831–12842.

Abdul Salim, N. A., Fulazzaky, M. A. & Muhammad, A. A. Z. S. 2021b Phosphate removal from wastewater in batch system using waste mussel shell. *Biointerface Research in Applied Chemistry* **11**(4), 11473–11486.

Aravind, M. & Amalanathan, M. 2021 Structural, morphological, and optical properties of country egg shell derived activated carbon for dye removal. *Materials Today: Proceedings* **43**(3), 1491–1495.

Azizian, S. 2004 Kinetic models of sorption: a theoretical analysis. *Journal of Colloid and Interface Science* **276**(1), 47–52.

Barakan, S., Aghazadeh, V. & Samiee Beyragh, A. 2020 Thermodynamic, kinetic and equilibrium isotherm studies of As(V) adsorption by Fe(III)-impregnated bentonite. *Environment, Development and Sustainability* **22**(2020), 5273–5295.

Barry, A. W. & James, A. F. 2016 Dewatering. In: *Wills' Mineral Processing Technology* (James A. Finch), Oxford, United Kingdom 8th edn. Elsevier, Butterworth-Heinemann.

Boyd, G. E., Adamson, A. W. & Myers, L. S. 1947 The exchange adsorption of ions from aqueous solutions by organic zeolites. II. Kinetics. *Journal of the American Chemical Society* **69**(11), 2836–2848.

Edet, U. A. 2020 Augustine OI. Kinetics, isotherms, and thermodynamic modeling of the adsorption of phosphates from model wastewater using recycled brick waste. *Processes* **8**(6), 665.

Efome, J. E., Rana, D. & Matsuura, T. 2018 Metal-organic frameworks supported on nanofibers to remove heavy metals. *Journal of Materials Chemistry* **10**(2018), 4550–4555.

Gilbert, A. S. 1999 IR spectral group frequencies of organic compounds. *Encyc. Spec. & Spectro.* **1999**, 1187–1198.

Ho, Y. S. 2006 Review of second-order models for adsorption systems. *Journal of Hazardous materials* **136**(3), 681–689.

Ho, Y. S. & McKay, G. A. 1998 Comparison of chemisorption kinetic models applied to pollutant removal on various sorbents. *Process Safety and Environment Protection* **76**(4), 332–340.

Huan, X., Qingqing, L. & Yan, Y. 2021 Highly effective removal of phosphate from complex water environment with porous Zr-bentonite alginate hydrogel beads: facile synthesis and adsorption behavior study. *Applied Clay Science* **201**(2021), 105919.

Jibing, X., Yong, Q. & Ejazul, I. 2011 Phosphate removal from solution using powdered freshwater mussel shells. *Desalination* **276**(1), 317–321.

Jung, K. W., Lee, S. Y. & Choi, J. W. 2021 Synthesis of Mg–Al layered double hydroxides-functionalized hydrochar composite via an in situ one-pot hydrothermal method for arsenate and phosphate removal: structural characterization and adsorption performance. *Chemical Engineering Journal* **420**(1), 129775.

Kun, W., Yang, L. & Ting, L. 2019 The simultaneous adsorption of nitrate and phosphate by an organic-modified aluminum manganese bimetal oxide: adsorption properties and mechanisms. *Applied Surface Science* **478**(1-2), 539–551.

Leone, M. & Vincenzo, P. 2020 *Fermentation and Biochemical Engineering: Principles and Applications*. Elsevier, New York, USA.

Li, R., Kelly, C. & Keegan, R. 2013 Phosphorus removal from wastewater using natural pyrrhotite. *Colloids and Surfaces A: Physicochemical and Engineering Aspects* **427**, 13–18.

Liu, Y. & Shen, L. 2008 Langmuir kinetics to first- and second-order rate equations for adsorption. *Langmuir* **24**(20), 11625–11630.

Malihe, A., Zahra, A. K. & Elnaz, E. 2019 Nitrate (NO_3^-) and phosphate (PO_4^{3-}) removal from aqueous solutions by microalgae Dunaliella salina. *Biocatalysis and Agricultural Biotechnology* **19**(2019), 101097.

Mengyuan, Z., Jingqi, D. & Rui, L. 2021 Two-period based carbon-economy equilibrium strategy for modular construction supply planning. *Journal of Cleaner Production* **290**(4), 125674.

Merenda, A., Ligneris, E. & Sears, K. 2016 Assessing the temporal stability of surface functional groups introduced by plasma treatments on the outer shells of carbon nanotubes. *Scientific Reports* **6**, 31565.

Nguyen, T. A. H., Ngo, H. H. & Guo, W. S. 2020 White hard clam (Meretrix lyrata) shells as novel filter media to augment the phosphorus removal from wastewater. *Science of the Total Environment* **741**(2020), 140483.

Nodeh, H. R., Sereshti, H. & Afsharian, E. Z. 2017 Enhanced removal of phosphate and nitrate ions from aqueous media using nanosized lanthanum hydrous doped on magnetic graphene nanocomposite. *Journal of Environmental Management* **197**, 265–274.

Norman, B. C., Lawrence, H. D. & Stephen, E. W. 1990 *Amines, C = N, and N = O Compounds, Introduction to Infrared and Raman Spectroscopy*, 3rd edn. Academic Press, London.

Payel, D. & Animesh, D. 2021 Reactive orange 12 dye adsorption onto magnetically separable $CaFe_2O_4$ nanoparticles synthesized by simple chemical route: kinetic, isotherm and neural network modelling. *Water Practice & Technology*. **16**, 1141–1158.

Peter, L. 2018 *General Outline for IR and Raman Spectral Interpretation. Infrared and Raman Spectroscopy*, 2nd edn. Elsevier, Amsterdam.

Qiu, H., Lv, L. & Pan, B. C. 2009 Critical review in adsorption kinetic models. *Journal of Zhejiang University-Science A* **10**(2009), 716–724.

Rafia, F., Tamino, H. & Detlef, K. 2021 Reaction of calcium carbonate minerals in sodium silicate solution and its role in alkali-activated systems. *Minerals Engineering* **165**(2021), 106849.

Rao, S. S. 2001 Theory of vibration | energy methods. *Encyclopedia of Vibration* **2001**, 1308–1324.

Salim, M., Asik J, R. & Sarjadi, M. S. 2021 Chemical functional groups of extractives, cellulose and lignin extracted from native Leucaena leucocephala bark. *Wood Science and Technology* **55**, 295–313.

Singh, N. B., Nagpal, G. & Agrawal, S. 2018 Water purification by using adsorbents: a review. *Environmental Technology & Innovation* **11**(2018), 187–240.

Suprakas, S. R., Rashi, G. & Neeraj, K. 2020 *Effect of Reaction Parameters on the Adsorption. In Micro and Nano Technologies, Carbon Nanomaterial-Based Adsorbents for Water Purification*. Elsevier, Amsterdam.

Tran, T. T., Tran, N. N. T., Sugiyama, S. & Liu, J. C. 2021 Enhanced phosphate removal by thermally pretreated waste oyster shells. *Journal of Material Cycles and Waste Management* **23**, 177–185.

Worch, E. 2012 *Adsorption Technology in Water Treatment*. De Gruyter, Boston.

Xie, Q., Li, Y. & Lv, Z. 2017 Effective adsorption and removal of phosphate from aqueous solutions and eutrophic water by Fe-based MOFs of MIL-101. *Scientific Reports* **7**, 3316.

Yuri, M. L. & Anatoliy, M. S. 2011 Synthesis, structure, chemical reactivity, and practical significance of 2-Amino-4H-pyrans. *Advances in Heterocyclic Chemistry* **103**(2011), 175–260.

First received 7 January 2022; accepted in revised form 6 May 2022. Available online 16 May 2022